DEVELOPMENT OF SANDBARS AROUND ISLANDS OFFSHORE OF KRABI IN THAILAND AND THEIR PREDICTION

Takaaki Uda[1], Masumi Serizawa[2] and Shiho Miyahara[2]

Poda and Po Da Nok Islands are located offshore of Krabi facing the Andaman Sea in the south part of Thailand. A shallow sea extends together with the development of a slender sandbar between these islands, and there is another small island named Tup Island connected by sandy beach. Sandbars can well develop in this area because of the shallow sea. The wave-sheltering effect of these islands affect to another island. On August 2016, field observation was carried out to study the formation of sandbars, and numerical simulation using the BG model was carried out to investigate the interaction of three islands.

Keywords: island; Krabi; sandbar; topographic changes; BG model; wave-sheltering effect

INTRODUCTION

When multiple islands composed of sand are located in a shallow sea, the wave-sheltering effect of one island affects the wave field around another island, and sandbars connecting these islands may develop because of their wave-sheltering effect. Serizawa et al. (2014) predicted the deformation of multiple, circular islands composed of sand located in a shallow flat sea. Assuming that waves were incident from all the directions between 0° and 360° with an equivalent probability of occurrence, they predicted the deformation of two circular islands. On the other hand, when waves are incident from two completely opposite directions, the connection or the merging of two sandbars can take place when a sandbar is subject to the wave-sheltering effect by another sandbar. Miyahara et al. (2018) predicted the extension of the sandbar between two islands using the BG model, taking multiple islands located in the southwestern part of Korea facing the Yellow Sea and those offshore of the coast facing the Kara Sea in Russia, together with five other islands in Korea and Japan as examples. In south part of Thailand, Poda and Po Da Nok Islands are located offshore of Krabi, facing the Andaman Sea, and a shallow sea extends offshore of these islands, and sandbars of characteristic shape extend between the islands. In addition, a small island named Tup Island is located between Poda and Po Da Nok Islands, in which two rocky islands, i.e., east and west islands, were combined by a sandbar. Since a shallow sea extends around these islands, sandbars well develop, and each island affects the wave field of the other island, forming sandbars of characteristic shape. In August 2016, field observation was carried out to investigate the mechanism of elongation of a sandbar between islands. Then, numerical simulation of topographic changes was carried out using the BG model which was used for the prediction of the deformation of a circular island (Serizawa et al. 2014).

DEVELOPMENT OF SANDBAR OFFSHORE OF KRABI IN THAILAND

Field observation was carried out on August 10, 2016 around the multiple islands located 5 km offshore of the Krabi resort to study the mechanism of formation of sandbars. Figure 1 shows a satellite image of the study area. The study area faces the Andaman Sea, and waves are incident from the SW during the southwest monsoon of rainy season and from the NE during the northeast monsoon of dry season. Yao Yai Island is located 23 km west of the study area, and Puket Island further 28 km west of the island. Although the study area is subject to the wave-sheltering effect by these islands, wave incidence from the sea between Phi Phi and Puket Islands is capable during the southwest monsoon. In contrast, wind waves which are generated over the fetch distance of 12.5 km are incident to these islands during the northeast monsoon. The wave height during the northeast monsoon is lower than that during the southwest monsoon because of the short fetch distance.

Figure 2 shows an enlarged satellite image of the rectangular area shown in Fig. 1. Poda and Po Da Nok Islands are located southwest of the Krabi resort with an interval of 1.2 km length. A submerged sandbar surrounded by coral reef extends from Poda Island to Po Da Nok Island. An enlarged satellite image of the rectangular area including Poda and Po Da Nok Islands is shown in Fig. 3. Although the submerged sandbar extends from Poda to Po Da Nok Islands, the sandbar extends for a distance of 1.1 km south of Poda Island, and then its direction changes southwestward near the Tup Island, which was connected by a sandbar between two small islands, and the sandbar further extends southwestward to reach the cuspate foreland at the north end of Po Da Nok Island.

[1] Public Works Research Center, 1-6-4 Taito, Taito, Tokyo 110-0016, Japan
[2] Coastal Engineering Laboratory Co., Ltd., 1-22-301 Wakaba, Shinjuku, Tokyo 160-0011, Japan

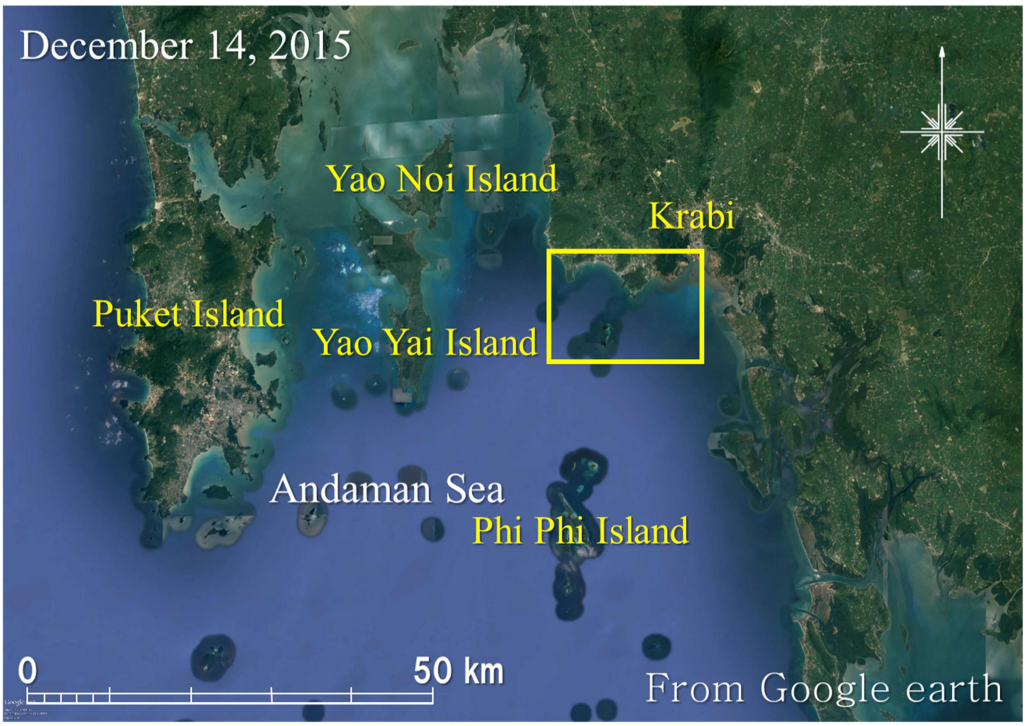

Figure 1. Study area offshore of Krabi in south part of Thailand.

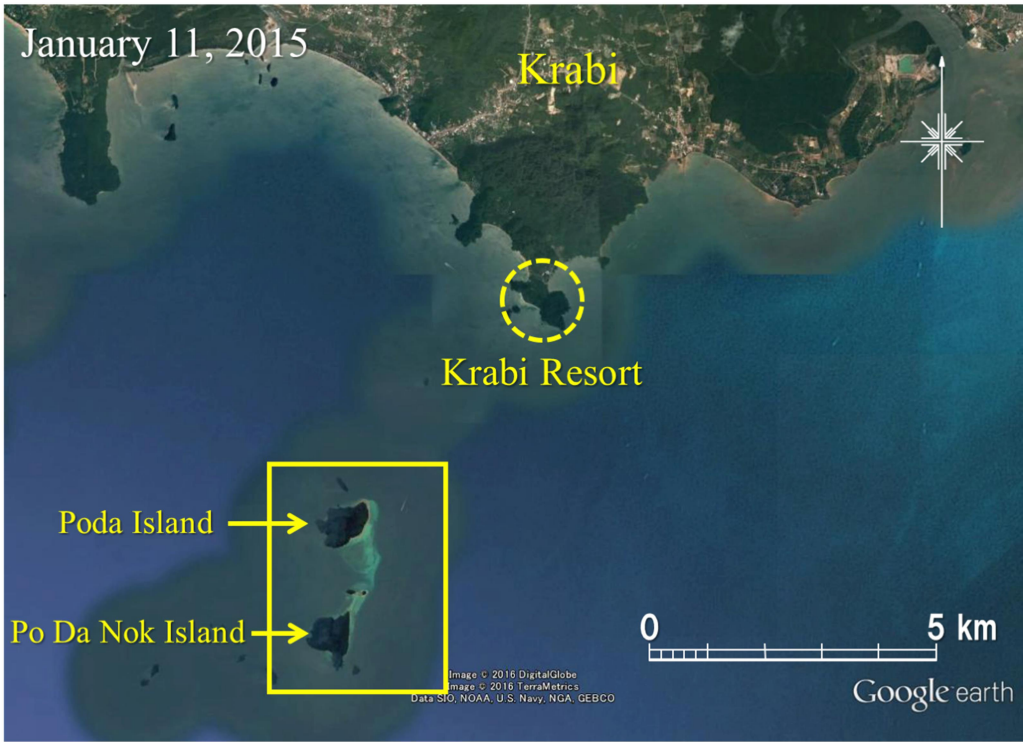

Figure 2. Satellite image of Poda and Po Da Nok Islands.

Figure 4 shows the enlarged satellite images of areas A and B in Fig. 3. Poda Island has a size of 930 and 740 m length in the east-west and south-north directions, respectively, and there exists no sandy beach on the west side of the island, whereas a sandy beach extends along the north and east shores of the island. Also, sand spits **a** and **b** are formed at the turning points of the coastline near the north and south ends of the island, respectively, and sandy beach continuously extends between these sand spits.

Similarly, there exists no sandy beaches on the west side of Po Da Nok Island except the pocket beach formed immediately west of a headland, and a narrow sandy beach extends along the east coast of the island. Thus, nonexistence of sandy beaches on the west side of the islands implies that the wave action during the southwest monsoon is intensive because of the long fetch distance, and sandy beach had been formed only on the east coast where the wave-sheltering effect by the island itself can be expected. At the same time, the fact that sand spits **a** and **b** develop westward on the east shore shows that easterly wave incidence predominated on January 11, 2016.

As for the development of a sandy beach in area B, as shown in Fig. 4, Tup Island is composed of two small islands, and a sandbar of 120 m length combines two small islands. In addition, another slender sandbar extends from Po Da Nok Island at an angle of 74° relative to the direction of the sandbar of Tup Island. Tup Island is located 780 m south of Poda Island, whereas Po Da Nok Island is distant from 260 m from Tup Island, being subject to greater wave-sheltering effect from Po Da Nok Island.

Figure 5 shows an enlarged satellite image of the sandbar extending northward from Po Da Nok Island and the sandy beach of Tup Island. A slender sandbar extends between two islands of Tup Island, and a cuspate foreland is formed at the north end of Po Da Nok Island which extends northeastward as a submerged sandbar. In Fig. 5, the location where site photographs were taken is also shown.

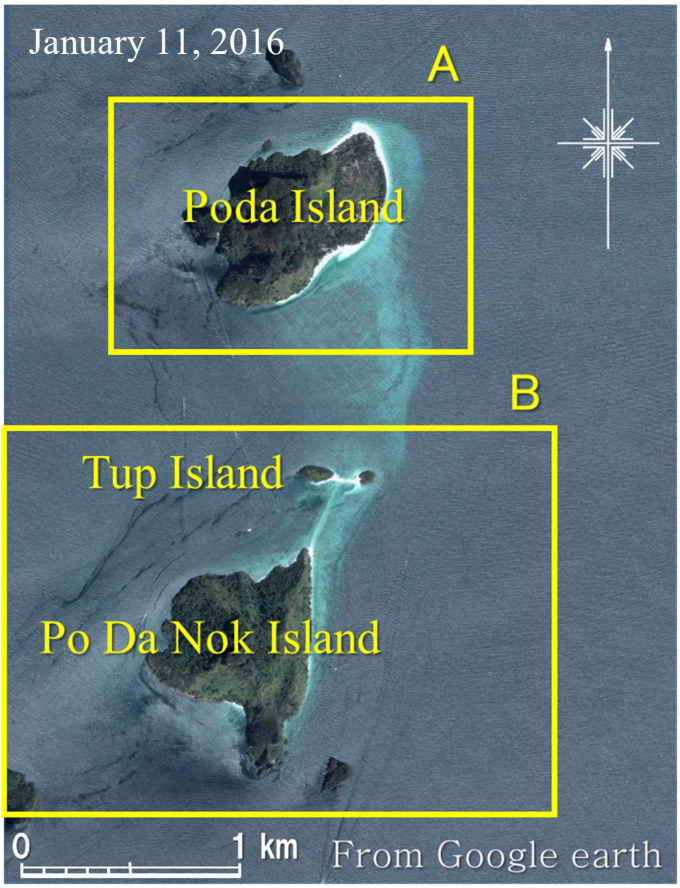

Figure 3. Enlarged satellite image of Poda and Po Da Nok Islands.

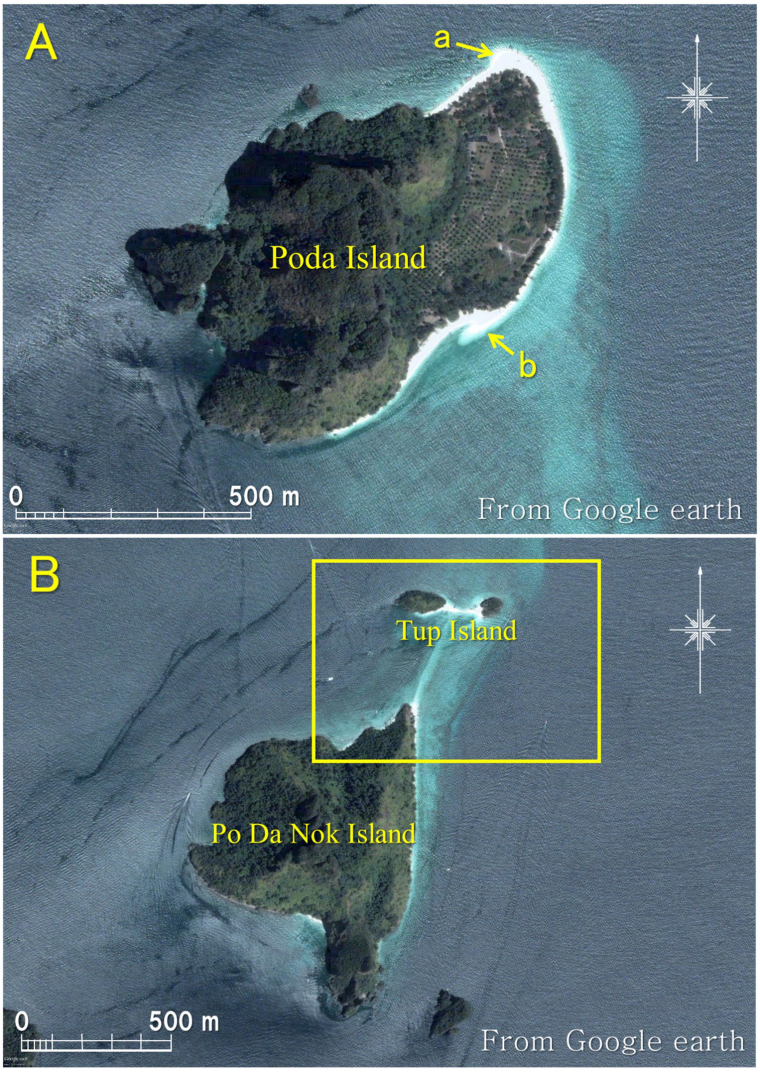

Figure 4. Sand spit of Poda Island and enlarged satellite image of Tup Island.

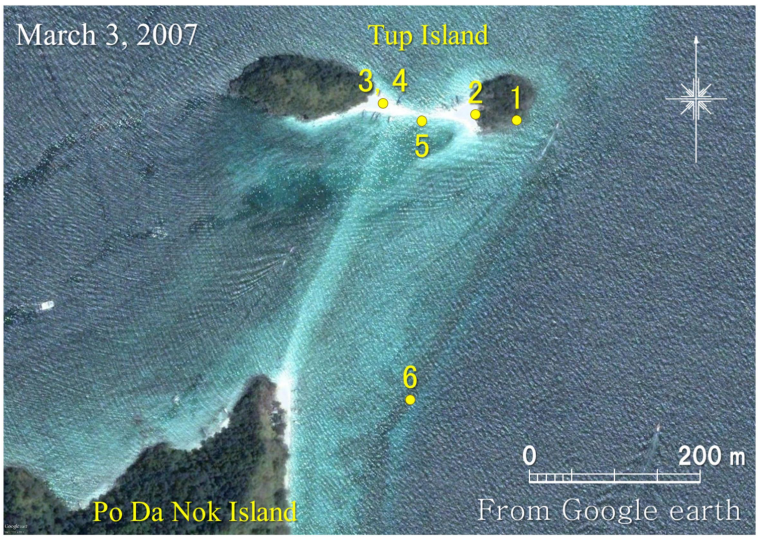

Figure 5. Location of site photographs around Tup Island.

FIELD OBSERVATION

We landed on Tup Island from the east side of east island. Figures 6 and 7 show a narrow sandy beach with a foreshore slope of 1/10 located at the eastern end of east island, and a slender sandy beach extending between east and west islands. The shoreline of the sandbar connecting both islands is concave on the northern side, as shown in Fig. 7, and many boats which transported many tourists from Krabi were moored there, because calm wave zone was formed. In contrast, many sea bathers gathered on the sandy beach on the south side. The height of sandbar was sufficiently high not to submerge during high tide. Figure 8 shows the condition of west island, and it was composed of hard limestone. Figure 9 shows the east island taken from the same point as that of Fig. 8. Figure 10 shows Po Da Nok Island taken from St. 5 on the south side of the sandbar. Many sea bathers on the submerged sandbar clearly suggest that a shallow sea extends between Tup and Po Da Nok Islands. Also, the existence of a cuspate foreland at the north end of Po Da Nok Island was confirmed. Figure 11 shows the cuspate foreland at the north end of the island, which was taken at a location 150 m east of Po Da Nok Island.

Figure 6. Narrow sandy beach formed at east end of Tup Island.

Figure 7. Sandy beach connecting two small islands of Tup Island.

Figure 8. East island and sandy beach looking from vicinity of west island.

Figure 9. East island looking from on sandy beach.

Figure 10. Po Da Nok Island looking from on south side of cuspate foreland.

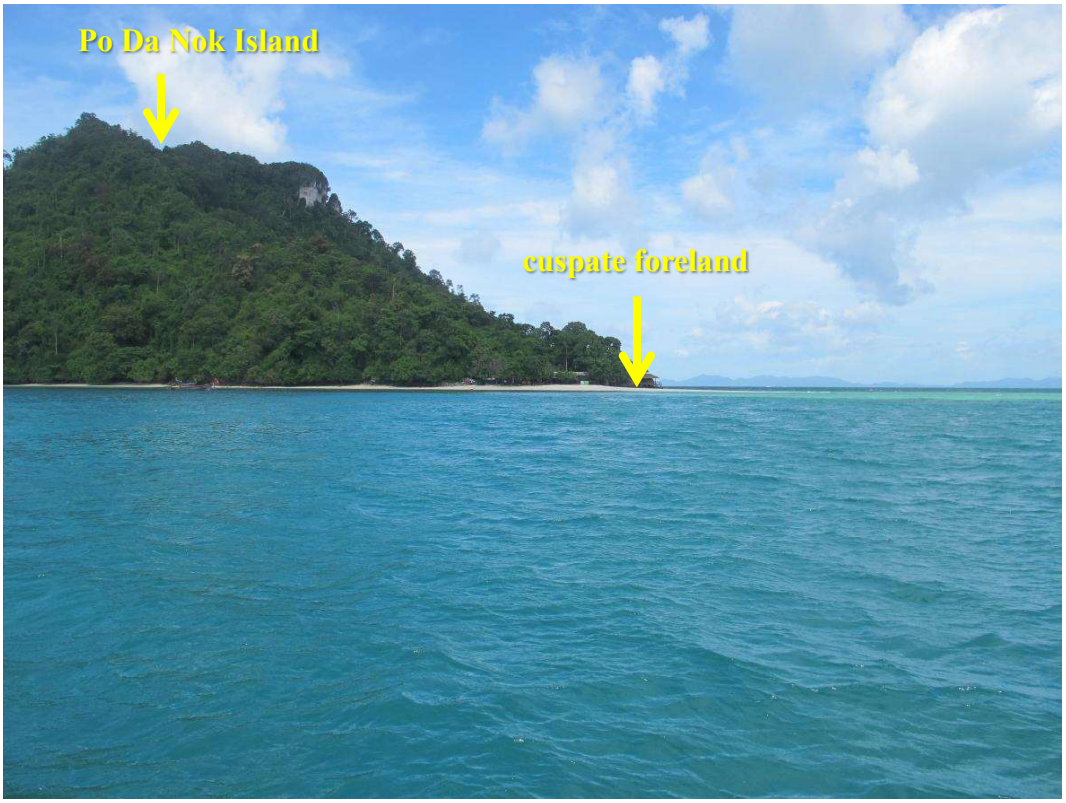

Figure 11. Cuspate foreland extending from north end of Po Da Nok Island.

PREDICTION OF EXTENSION OF SANDBARS CONNECTING MULTIPLE ISLANDS

The sand transport equation employed in this study is Eq. (1), using the expression of the wave energy evaluated at the breaking point, the same as in the BG model proposed by San-nami et al. (2013), and Serizawa et al. (2014), and is equal to the Type 5 BG model in Uda et al. (2018). The variables in Eq. (1) are given by Eqs. (2) - (5).

$$\vec{q} = C_0 \frac{K_s P}{\tan\beta_c}\left\{\tan\beta_c \vec{e}_w - |\cos\alpha|\ \overrightarrow{\nabla Z}\right\} \qquad (-h_c \le Z \le h_R) \tag{1}$$

$$P = \varepsilon\,(Z)\ (EC_g)_b \tan\beta_w \qquad (P \ge 0) \tag{2}$$

$$\tan\beta_w = dZ/dx_w \qquad (\tan\beta_w \ge 0) \tag{3}$$

$$\int_{-h_c}^{h_R} \varepsilon\,(Z)\,dZ = 1 \tag{4}$$

$$\varepsilon\,(Z) = \begin{cases} \dfrac{1}{h_c + h_R} & (-h_c \le Z \le h_R) \\ 0 & (Z < -h_c,\ \ Z > h_R) \end{cases} \tag{5}$$

$$(EC_g)_b = C_1 (H_b)^{\frac{5}{2}} \approx C_1 (H_{1/3})^{\frac{5}{2}} \tag{6a}$$

$$C_1 = \frac{\rho g}{k_1}\sqrt{g/\gamma} \qquad \left(\ k_1 = (4.004)^2,\ \ \gamma = 0.8\ \right) \tag{6b}$$

Here, $\vec{q} = (q_x, q_y)$ is the net sand transport flux, Z (x, y, t) is the seabed elevation with reference to the still water level ($Z = 0$), $\overrightarrow{\nabla Z} = (\partial Z/\partial x,\ \partial Z/\partial y)$ is the seabed slope vector, $\vec{e}_w$ is the unit vector of wave direction, α is the angle between the wave direction and the direction normal to the contour line, x_w is

the coordinate along the direction of wave propagation, $\tan\beta_w$ is the seabed slope measured along the direction of wave propagation, $\tan\beta_c$ is the equilibrium slope of sand, and K_s is the longshore and cross-shore sand transport coefficient. C_0 is the coefficient transforming the immersed weight expression to the volumetric expression ($C_0 = 1/\{(\rho_s - \rho)g(1-p)\}$; ρ is the seawater density, ρ_s is the specific gravity of sand, p is the porosity of sand, and g is the acceleration due to gravity), h_c is the depth of closure, and h_R is the berm height.

In the calculation, the local beach slope measured along the wave ray was used as the beach slope in Eq. (2), as shown in Eq. (3). $\varepsilon(Z)$ in Eq. (5) is the depth distribution of sand transport, $(EC_g)_b$ is the wave energy flux at the breaking point, H_b is the breaker height, $H_{1/3}$ is the significant wave height of the incident waves, and γ is the ratio of the breaker height relative to the water depth. In addition, $k_1 = (4.004)^2$ in Eq. (6b) is a constant in the relationship between the wave energy E and the significant wave height when the probability of the wave height of irregular waves is assumed to be given by the Rayleigh distribution (Horikawa 1988).

For the calculation of the P value in Eq. (2), another coordinate system different from that for the calculation of beach changes was used (San-nami et al. 2013; Uda et al. 2018), in which the x_w- and y_w-axes were taken along the wave direction and the direction normal to that, respectively (Fig. 12). A fixed coordinate system of (x, y) is for the calculation of beach changes with a calculation domain of a rectangular ABCD, whereas the P value was calculated in the rectangular domain of A'B'C'D' including the domain ABCD with the coordinate system of (x_w, y_w). In the wave calculation, wave refraction was neglected and waves were assumed to propagate in a straight manner while maintaining wave incident angle.

The distance along the x_w-axis is subdivided by the mesh of Δx_w, and a cumulative function of $\varepsilon(Z)$, $I_\varepsilon(Z)$, is introduced as Eq. (7). Here, $\varepsilon(Z)$ is assumed to have a uniform distribution (Eq. (5)) and $I_\varepsilon(Z)$ is a function that takes unity in a zone deeper than the depth of closure, decreases with the water depth, and becomes 0 in a zone higher than the berm height. Using Eq. (7), Eq. (2) is transformed into Eq. (8). Thus, the P value can be determined from the derivative of $I_\varepsilon(Z)$ at a point along the x_w-axis using Eq. (8). The index i in Eqs. (9) and (10) is the mesh number along the x_w-axis, and min means the selection of the smaller of either value in parentheses.

$$I_\varepsilon(Z) = \begin{cases} 1 & (Z < -h_c) \\ \displaystyle\int_Z^{h_R} \varepsilon(Z)\, dZ = \frac{h_R - Z}{h_c + h_R} & (-h_c \le Z \le h_R) \\ 0 & (Z > h_R) \end{cases} \tag{7}$$

$$P = (EC_g)_b \left(-\frac{dI_\varepsilon}{dx_w} \right) \qquad (P \ge 0) \tag{8}$$

$$I_\varepsilon^{(i+1)} = \min\left(\text{Eq. (7)} \Big|^{Z=Z^{(i+1)}},\ I_\varepsilon^{(i)} \right) \tag{9}$$

$$P^{(i+1/2)} = (EC_g)_b \left(\frac{I_\varepsilon^{(i)} - I_\varepsilon^{(i+1)}}{\Delta x_w} \right) \tag{10}$$

$I_\varepsilon(Z)$ is calculated along the x_w-axis from the starting point of wave incidence toward the direction of wave propagation; $I_\varepsilon(Z)$ at the $(i+1)^{th}$ point can be calculated from Eq. (9) with the given value of $I_\varepsilon(Z)$ at the i^{th} point, when the initial value of $I_\varepsilon(Z)$ at the offshore end is given and the mesh location is denoted by $x_w^{(i)} = i\Delta x_w$.

Furthermore, the P value at the $(i+1/2)^{th}$ point is calculated from Eq. (10) which is the derivative expression of Eq. (8). Note that in calculating $I_\varepsilon(Z)$ at the $(i+1)^{th}$ point, the smaller value between the one calculated from Eq. (7) given the elevation $Z(i+1)$ at the $(i+1)^{th}$ point and $I_\varepsilon(Z)$ at the i^{th} point is adopted. As a result, the value of $I_\varepsilon(Z)$ corresponding to the minimum water depth (maximum Z) between the offshore end to a designated point along the x_w-axis can be adopted. Using this procedure, the depth distribution along the x_w-axis between the offshore end and a certain point is automatically taken into account in the calculation of the P value.

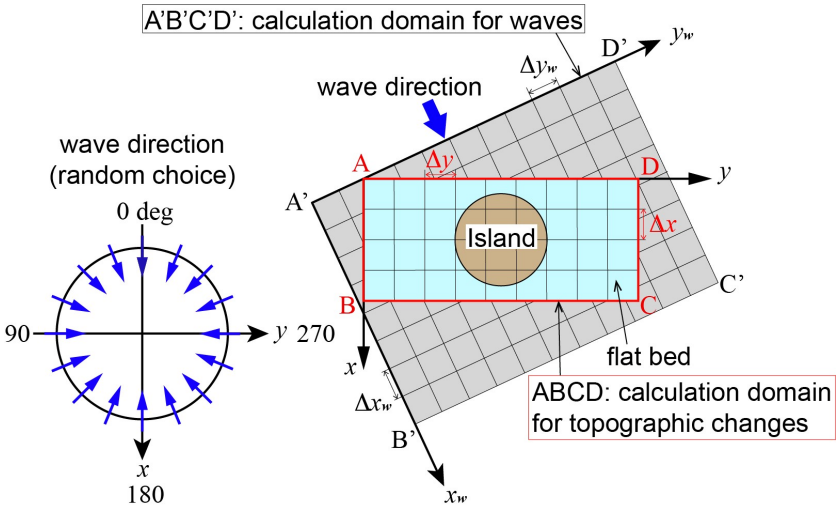

Figure 12. Definition of coordinate system around an island.

In addition, the P value integrated from a location on land where the elevation exceeds the berm height to an offshore end along the x_w-axis is always equivalent to the wave energy flux at the breaking point $(EC_g)_b$ with no regard to the seabed topography. Because $(EC_g)_b$ corresponds to the entire power of the incident waves, the exact satisfaction of this condition is reasonable.

The calculation of the P value is independently carried out along each x_w-axis. The P value calculated at a point of (x_w, y_w) is memorized, and the P value at a point of (x, y) necessary for the calculation of beach changes was interpolated from the memorized value at a point of (x_w, y_w). The mesh intervals of Δx_w and Δy_w are the same as those of Δx and Δy. Here, Δx and Δy are the mesh intervals of the coordinate system for the calculation of beach changes, and we assumed the equivalent condition of $\Delta x = \Delta y$. The beach changes were calculated by explicitly solving the continuity equations ($\partial Z/\partial t + \nabla \bullet \vec{q} = 0$) on the staggered meshes using the sand transport fluxes obtained from Eq. (1). The P value, which is subject to change with the propagation of waves, was recalculated at every calculation step of beach changes. In addition, when the ground elevation Z approaches the upper limit (h_R) or the lower limit of beach changes ($-h_c$) in the calculation process of beach changes, the sand transport rate was reduced by multiplying the reduction ratio using the method of Uda et al. (2013), so that the beach changes over these limits do not occur.

In estimating the intensity of sand transport near the berm top and at the depth of closure, the intensity of sand transport was linearly reduced to 0 near the berm height or the depth of closure to prevent sand from being deposited in the zone higher than the berm height and the beach from being eroded in the zone deeper than the depth of closure, as described by Uda et al. (2013). Although the wave height was assumed to be constant, the probability distribution of occurrence of the wave direction was given in this study. The wave direction at each time step was given by a single value by random number so as for the wave direction to satisfy the probability distribution, assuming that the wave direction has an equivalent probability of occurrence from all the directions between 0° and 360°. The distribution of P value was recalculated after the wave direction was reset by random number every one step of beach changes. Further detail of the calculation method can be found in Uda et al. (2018).

CALCULATION CONDITIONS

The Cartesian coordinates (x, y) were adopted, as shown in Fig. 13, and a rectangular area with 1.2 km length in the x- and y- directions was adopted as a calculation domain. Since a shallow sea extends around Tup Island, the water depth was set to be 2 m in the calculation domain, and a solid bed was assumed. Two cases of the calculation were carried out, as shown in Fig. 13 with changing the arrangement and number of islands: in Case 1, two circular islands were set as a model of the west and east islands of Tup Island, and topographic changes associated with the elongation of sandbars were predicted. The radii of the circular islands were determined to be 60 and 40 m in the west and east islands, respectively, taking into account that the shape of the island is oval, and the length of the principal axis of the west island is 160 m longer than the 80 m length of the east island comprising Tup

Island. The core of the island was assumed to be made of rocks, as shown in Figs. 8 and 9, and a sandy beach with the berm height of 1 m and the beach slope of 1/10 extends around the model islands. In Case 2, third circular island composed of sand was placed on the south side in addition to the condition in Case 1. Under this condition, a slender sandbar may extend northward from the sand source at the north end of Po Da Nok Island located south of Tup island to connect the sandbar between east and west islands of Tup Island. In the calculation, a circular, sandy island, the third island, was placed, to model the effect of the sand source at the north end of Po Da Nok Island. In Case 2, taking the wave-sheltering effect owing to Po Da Nok Island into account, the development of a slender sandbar extending from Po Da Nok Island to Tup Island was predicted. Waves of significant wave height of 1 m were assumed to be incident from all the direction between 0° and 360° around the calculation domain with an equivalent intensity. The wave direction at each step in the calculation of beach changes was selected to be a value determined by random numbers so as to satisfy the probability distribution function of the occurrence of a certain wave direction. Table 1 shows the calculation conditions.

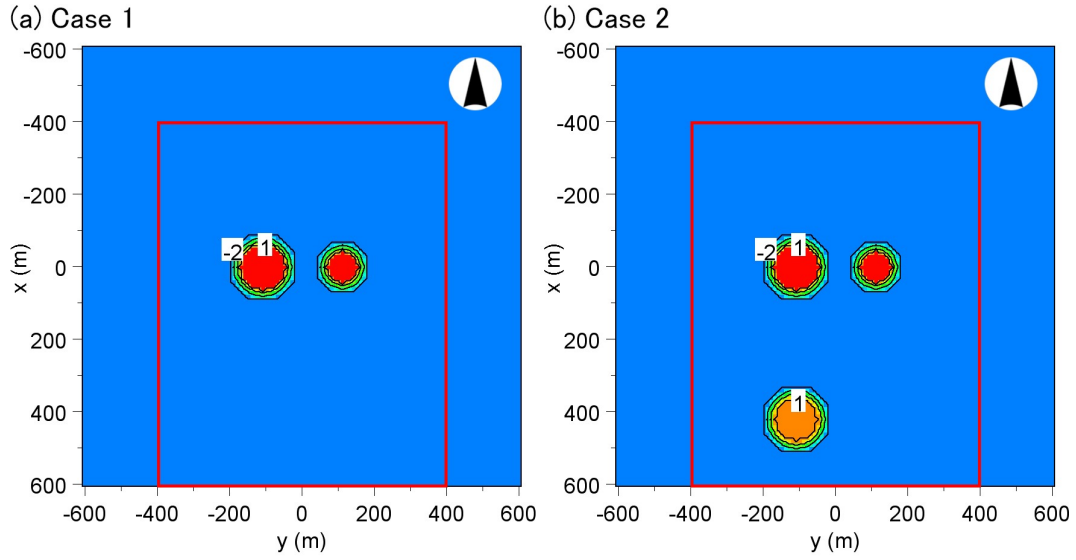

Figure 13. Coordinates for calculation and arrangement of islands in Cases 1 and 2.

Table 1. Calculation conditions.	
Incident wave height H	H = 1 m
Berm height h_R	1 m
Depth of closure h_c	2 m
Equilibrium slope tanβ_c	1/10
Coefficient of sand transport	K_s = 0.2
Mesh size	$\Delta x = \Delta y$ = 10 m
Time intervals	Δt = 1 h
Duration of calculation	1×10^4 h (1×10^4 steps)

CALCULATION RESULTS

Figure 14 shows the calculation results in Case 1. A sandbar started forming between the east and west islands located with an opening length of 120 m at first because of the wave-sheltering effect of each other's island. By 2,000 steps, a straight sandbar extended between two islands, similarly to Tup Island, and the shape of the sandbar has almost stable form up to this step, and no large beach changes occurred after 3,000 steps. This well explain the formation process of a sandbar between two small islands of Tup Island, as shown in Fig. 5. Similarly, Fig. 15 shows the results of Case 2, in which south island modeled the sand source at the north end of Po Da Nok Island was placed together with Tup Island. Since the shape of west and east islands of Tup Island is the same as that in Case 1, a slender sandbar extended between two small islands, similarly to that in Case 1. In Case 2, however, south island is located south of west and east islands, and intensive wave-sheltering effect of this island reached to the west island, a cuspate foreland started to develop at the south end of the west island.

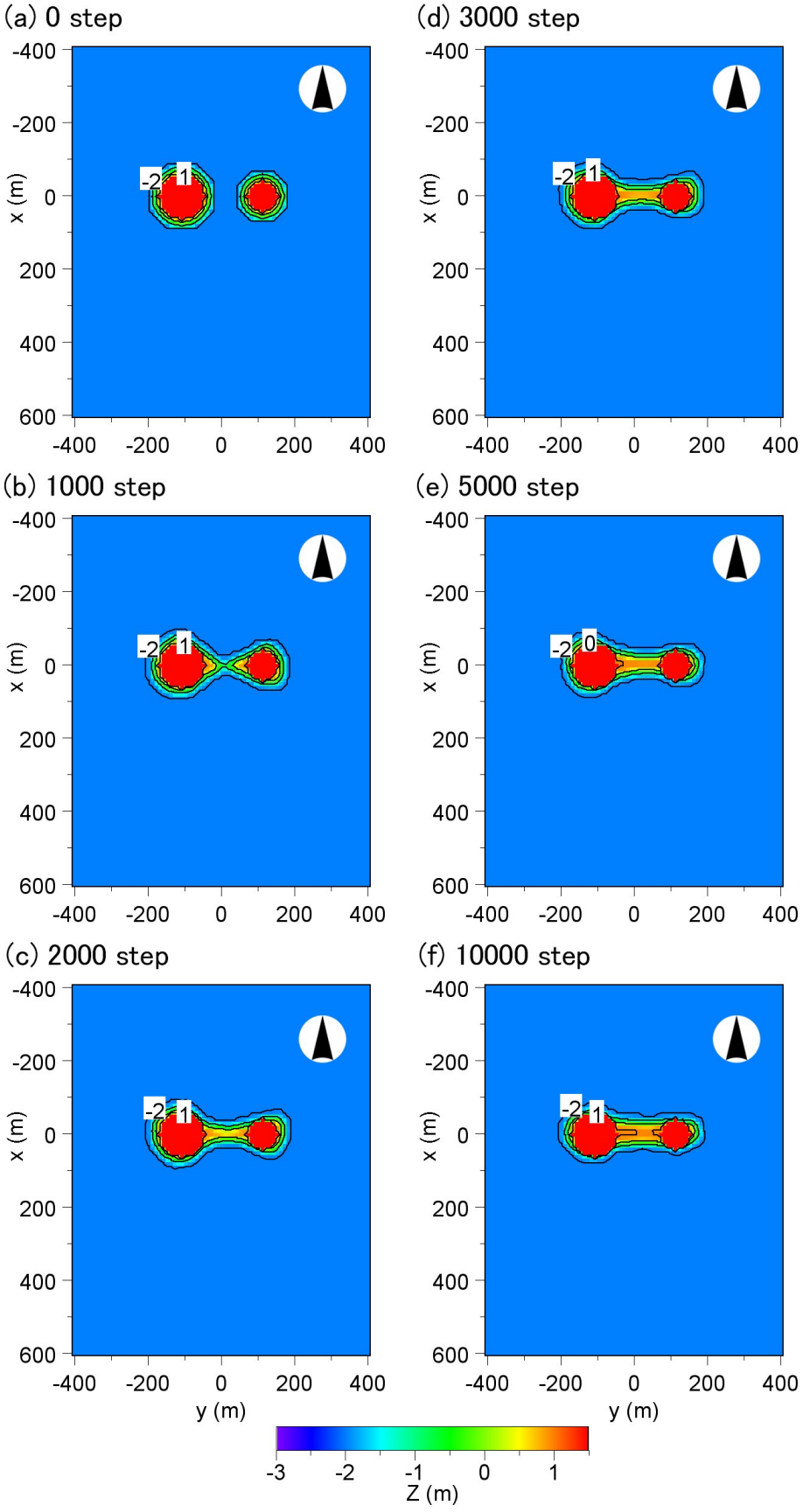

Figure 14. Calculation results in Case 1.

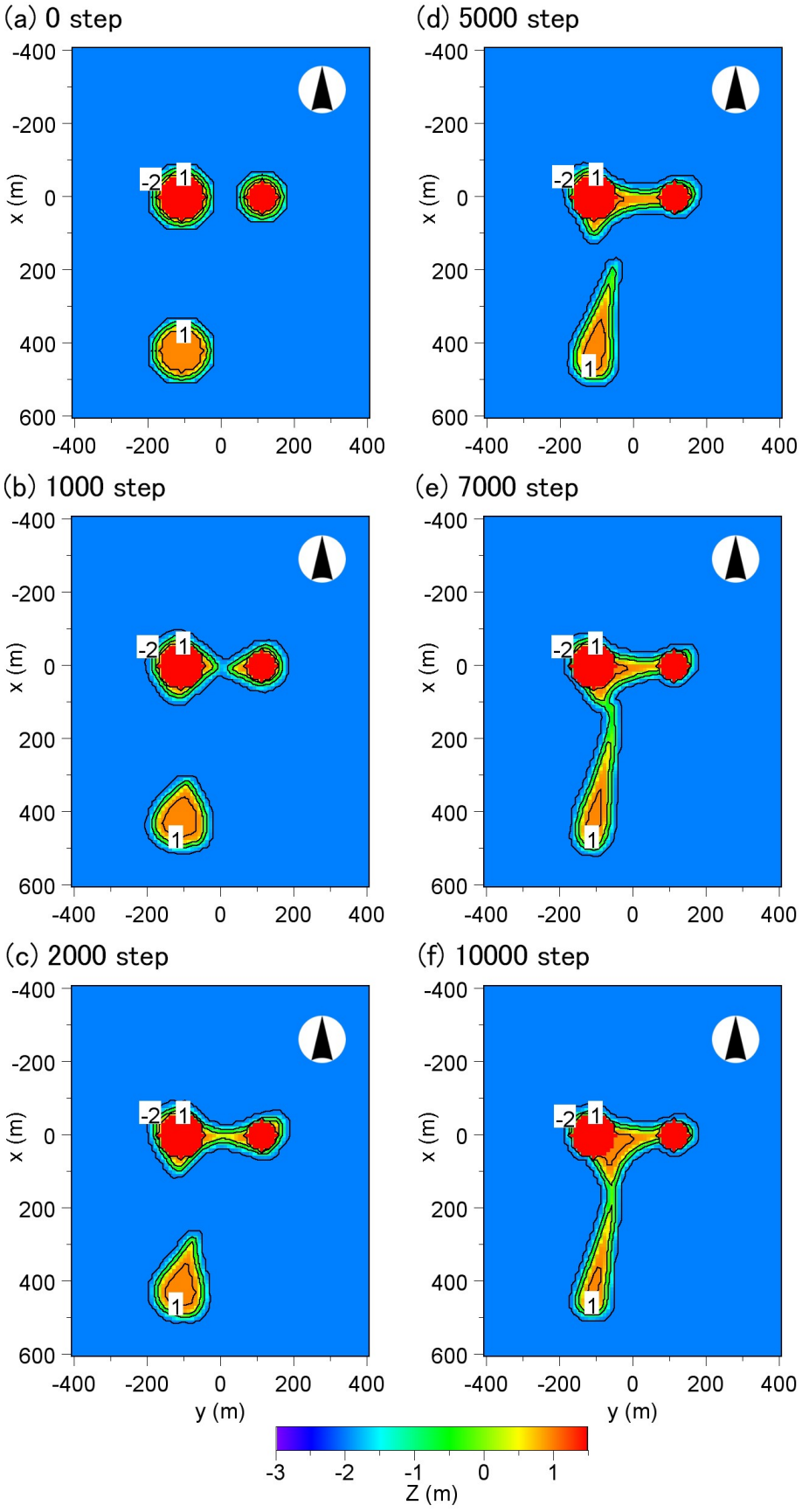

Figure 15. Calculation results in Case 2.

Because the south island was simultaneously subject to the wave-sheltering effect by the west and east islands, another cuspate foreland started to extend northward. After 2,000 steps, this cuspate foreland further extended to approach to the vicinity of west and east islands, and after 7,000 steps, south island connected to the west island by a slender sandbar. Finally, after 1×10^4 steps, three islands connected each other by slender sandbars. This well explains the topographic changes, the extension of a sandbar between Tup Island and Po Da Nok Island, as shown in Figs. 5 and 10.

CONCLUSIONS

The mechanism of elongation of sandbars between islands extending between Poda and Po Da Nok Islands offshore of Krabi in Thailand was investigated by field observation in August 2016. Since a shallow sea extends around these islands, sandbars well develop, and each island affects the wave field of the other island, forming sandbars of characteristic shape. Then, numerical simulation of topographic changes was carried out using the BG model. It was concluded that sandbars extended between the islands due to the wave-sheltering effect of the islands.

REFERENCES

Horikawa, K. ed. 1988. *Nearshore Dynamics and Coastal Processes*, University of Tokyo Press, Tokyo, 522 p.

Miyahara, S., T. Uda, and M. Serizawa. 2018. Interaction and merging of cuspate forelands formed at end of multiple sandy islands under waves, *Proceedings of 36th International Conference on Coastal Engineering*, ASCE.

San-nami, T., T. Uda, M. Serizawa, and S. Miyahara. 2013. Prediction of devastation of natural coral cay by human activity, *Proceedings of Coastal Dynamics* 2013, Paper No. 138, 1427-1438.

Serizawa, M., T. Uda, and S. Miyahara. 2014. Interaction between two circular sandy islands on flat shallow seabed owing to waves, *Proceedings of 34th International Conference on Coastal Engineering*, ASCE, 1-12.
https://icce-ojs-tamu.tdl.org/icce/index.php/icce/article/view/7106/pdf_410

Uda, T., M. Gibo, T. Ishikawa, S. Miyahara, T. San-nami, and M. Serizawa. 2013. Change in carbonate beach triggered by construction of a bridge on Irabu Island and its simulation using BG model, Asian and Pacific Coasts 2013, *Proceedings of 7th International Conference*, 24-31.

Uda, T., M. Serizawa, and S. Miyahara. 2018. *Morphodynamic model for predicting beach changes based on Bagnold's concept and its applications*, INTEC, London, UK.
Doi: http://dx.doi.org/10.5772/intechopen.81411